

## Identification of a Corroded Boundary and its Robin Coefficient

B. Bin-Mohsin<sup>1,2</sup> and D. Lesnic<sup>1,\*</sup>

<sup>1</sup> Department of Applied Mathematics, University of Leeds, Leeds LS2 9JT, UK.

<sup>2</sup> Department of Mathematics, King Saud University, P.O. Box 4341, Riyadh 11491, Saudi Arabia.

Received 13 February 2012; Accepted (in revised version) 30 March 2012

Available online 27 April 2012

---

**Abstract.** An inverse geometric problem for two-dimensional Helmholtz-type equations arising in corrosion detection is considered. This problem involves determining an unknown corroded portion of the boundary of a two-dimensional domain and possibly its surface heat transfer (impedance) Robin coefficient from one or two pairs of boundary Cauchy data (boundary temperature and heat flux), and is solved numerically using the meshless method of fundamental solutions. A nonlinear unconstrained minimisation of the objective function is regularised when noise is added into the input boundary data. The stability of the numerical results is investigated for several test examples, with respect to noise in the input data and various values of the regularisation parameters.

**AMS subject classifications:** 65N20, 65N21, 65N80

**Key words:** Helmholtz-type equations, inverse problem, method of fundamental solutions, regularisation.

---

### 1. Introduction

Inverse geometric problems arise in analysing various imaging and tomography techniques such as electrical impedance tomography (EIT), gamma ray emission tomography (GRET), magneto-resonance imaging (MRI), etc. In this study, we consider the application of the method of fundamental solutions (MFS) to solve numerically the inverse geometric problem, which consists of determining an unknown part of the boundary  $\Gamma_2 \subset \partial\Omega$  assuming that the dependent variable  $u$  satisfies the Helmholtz (or the modified Helmholtz) equation in a simply-connected bounded domain  $\Omega \subset \mathbb{R}^2$  — viz.

$$\nabla^2 u \pm k^2 u = 0 \quad \text{in } \Omega \quad (1.1)$$

---

\*Corresponding author. Email addresses: mmbbm@maths.leeds.ac.uk (B. Bin-Mohsin), amt51d@maths.leeds.ac.uk (D. Lesnic)

where  $k > 0$ , from the knowledge of the Dirichlet boundary data  $u|_{\Gamma_1}$  and the Neumann flux data  $\partial u/\partial n$  — i.e. Cauchy data, on the known part of the boundary  $\Gamma_1 = \partial\Omega \setminus \Gamma_2$  where  $\underline{n}$  is the outward unit normal to the boundary, together with a boundary condition (Dirichlet, Neumann or Robin) on the unknown part of the boundary  $\Gamma_2$ . Eq. (1.1) with minus sign is the modified Helmholtz equation that models the heat conduction in a fin (e.g. [22]), whilst equation (1.1) with plus sign is the Helmholtz equation that models wave propagation in acoustics. The inverse, nonlinear and ill-posed problem of determining the unknown (inaccessible) corroded portion of the boundary  $\Gamma_2$  and possibly its surface heat transfer coefficient, if a Robin condition is prescribed on  $\Gamma_2$ , is approached using an MFS regularised minimisation procedure. This study is general and builds upon previous recent applications of the MFS to solve similar boundary determination corrosion problems for the isotropic, anisotropic and functionally graded Laplace equation [20, 24, 26, 27, 32], Helmholtz-type equations [23], the biharmonic equation [33], the Lamé system in elasticity [21], and the heat equation [10]. For more details about the MFS, as applied to inverse problems in general, see the recent review by Karageorghis *et al.* [15]. We finally mention that there also exists an extensive literature on using the boundary element method (BEM) instead of the MFS for the corrosion boundary identification — e.g. see [17] for the Laplace equation in EIT, [25] for the Lamé system in elasticity, and [19] for Helmholtz-type equations. However, there are clear methodological differences between the MFS and the BEM — e.g. see [1] for a comparison between the two methods. In summary, although the MFS formulation may introduce some extra ill-conditioning, by avoiding the numerical integration it is considerably easier to use, especially in higher dimensional problems.

The outline of this paper is as follows. In Section 2 we introduce and discuss the mathematical formulation, whilst in Section 3 we present the MFS for the Helmholtz-type equations. In Section 4 we present and discuss the numerically obtained results, and in Section 5 we give some conclusions and suggest possible future work.

## 2. Mathematical Formulation

We consider a simply-connected solution domain  $\Omega$  bounded by a smooth or piecewise smooth curve  $\partial\Omega = \Gamma_1 \cup \Gamma_2$ , where  $\Gamma_1 \cap \Gamma_2 = \emptyset$  and both  $\Gamma_1$  and  $\Gamma_2$  are of positive measure. The function  $u$  satisfies the Helmholtz (or the modified Helmholtz) equation (1.1) subject to the boundary conditions

$$u = f \quad \text{on } \Gamma_1 \quad (2.1)$$

and

$$\frac{\partial u}{\partial n} + \alpha u = h \quad \text{on } \Gamma_2, \quad (2.2)$$

where  $f \in H^{1/2}(\partial\Omega)$  non-constant and  $h \in H^{-1/2}(\partial\Omega)$  are given functions, and  $\alpha \in L^\infty(\Gamma_2)$  is the non-negative impedance (surface heat transfer) Robin coefficient. Here

$H^{1/2}(\partial\Omega)$  denotes the space of traces of functions  $u \in H^1(\Omega)$  restricted to the boundary  $\partial\Omega$ , and  $H^{-1/2}(\partial\Omega)$  denotes the dual space of  $H^{1/2}(\partial\Omega)$ . In Eq. (2.2),  $h$  is usually zero, in which case (2.2) represents a homogeneous Robin boundary condition. In the case of the Helmholtz equation we also assume that  $k^2$  is not an eigenvalue for the negative of the Laplacian  $-\nabla^2$  in the domain  $\Omega$  with the homogeneous form of the mixed boundary conditions (2.1) and (2.2) on  $\partial\Omega$ . It is well-known that the direct Robin problem given by Eqs. (1.1), (2.1) and (2.2) has a unique solution  $u \in H^1(\Omega)$  when  $\Gamma_2$  is known. We can then define a nonlinear operator  $F_f(\Gamma_2)$ , which maps the set of admissible Lipschitz boundaries  $\Gamma_2$  to the data space of Neumann flux data in  $H^{-1/2}(\Gamma_1)$ , as follows:

$$F_f(\Gamma_2) := \left. \frac{\partial u}{\partial n} \right|_{\Gamma_1} = g \in H^{-1/2}(\Gamma_1). \quad (2.3)$$

The inverse problem under consideration then consists of extracting some information about the boundary  $\Gamma_2$  from the data  $g = F_f(\Gamma_2)$ . The data (2.3) may also only be partial — i.e. the flux being measured on a non-zero measure portion  $\Gamma \subset \Gamma_1$ , instead of the whole boundary  $\Gamma_1$ . It is well-known that this inverse problem is nonlinear and ill-posed, as opposed to the direct problem that is linear and well-posed. The Robin boundary condition (2.2) models Newton's law of cooling, which gives a linear relationship between the heat flux and the surface temperature through a surface heat transfer (impedance) coefficient of proportionality  $\alpha$ .

We briefly note that the situation regarding the solution uniqueness or non-uniqueness is much more settled in the case of the inverse shape boundary determination of  $\Gamma_2$  when  $\alpha$  is known [4–6, 12, 13], or in the case of the inverse impedance determination of  $\alpha$  when  $\Gamma_2$  is known [7, 11, 14]. However, in corrosion problems it is not always physically realistic to assume that the boundary condition on the corroded boundary is known, in which case the coefficient  $\alpha$  in (2.2) together with the obstacle  $\Gamma_2$  are to be determined simultaneously. Clearly, one set of Cauchy boundary measurements (2.1) and (2.3) is then insufficient to recover  $\Gamma_2$  and  $\alpha$  simultaneously. However, it turns out that two linearly independent boundary data  $f_1$  and  $f_2$ , one of which is positive and inducing two corresponding flux measurements  $g_1$  and  $g_2$  via (2.3), are sufficient to provide a unique solution for the pair  $(\Gamma_2, \alpha)$  [2, 28, 29]. Recently, the stability issue has also been addressed [31]. Finally, we note that the case when  $\Omega$  is a doubly-connected annular domain with outer boundary  $\Gamma_1$  and inner unknown boundary  $\Gamma_2$  has also recently been investigated by the present authors [18].

Even when  $\alpha$  is known, one set of Cauchy data (2.1) and (2.3) may not be enough to determine uniquely the corroded boundary  $\Gamma_2$ , as the following counterexample shows:

#### **Counterexample.**

We extend the analysis of Ref. [5] for the Laplace equation (i.e. when  $k = 0$ ), and likewise consider the geometrical configuration for the solution domain  $\Omega$  sketched in Fig. 1 where

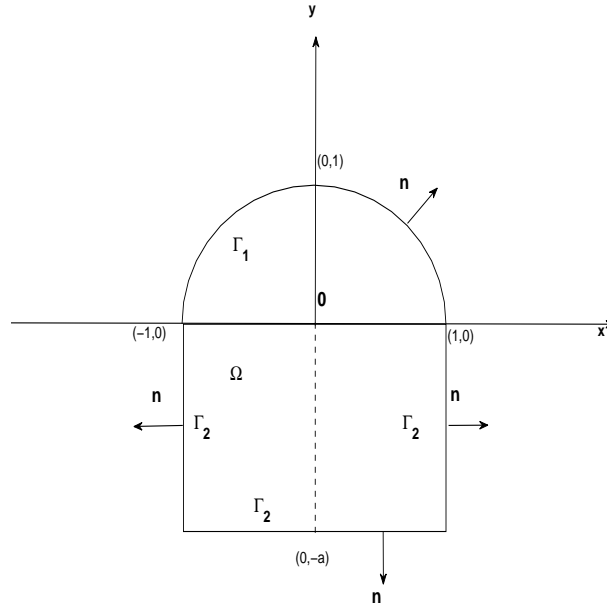


Figure 1: Geometry for the counterexample.

$a > 0$  is a constant parameter. Thus let the solution domain be

$$\Omega = \{(x, y) \in \mathbb{R}^2 \mid x^2 + y^2 < 1, y > 0\} \cup \{(x, y) \in \mathbb{R}^2 \mid x \in (-1, 1), y \in (-a, 0)\}, \quad (2.4)$$

consisting of a semicircle and a rectangle. Consider the function

$$u(x, y) = \sqrt{2}e^{\gamma y} \sin\left(\frac{\pi}{4}(\beta x + \beta + 1)\right), \quad (x, y) \in \Omega, \quad (2.5)$$

where  $\beta$  and  $\gamma$  are some constants to be prescribed.

(a) *The modified Helmholtz equation*

Let us first consider the case of the modified Helmholtz equation

$$\nabla^2 u - k^2 u = 0 \quad \text{in } \Omega. \quad (2.6)$$

It can be seen that (2.5) satisfies the modified Helmholtz equation (2.6) if  $\gamma^2 = k^2 + \beta^2 \pi^2 / 16$ . Let us now try to satisfy the homogeneous form of the Robin boundary condition (2.2) on  $\Gamma_2$ . On the left vertical boundary of  $\Gamma_2$  we have

$$\begin{aligned} u(-1, y) &= e^{\gamma y}, \\ \frac{\partial u}{\partial n}(-1, y) &= -\frac{\partial u}{\partial x}(-1, y) = -\frac{\pi\beta}{4}e^{\gamma y}, \quad y \in (-a, 0), \end{aligned}$$

and we can take

$$\alpha(-1, y) = \frac{\beta\pi}{4}, \quad y \in (-a, 0) \quad (2.7)$$

that we can make non-negative by requiring  $\beta \geq 0$ . On the right vertical boundary of  $\Gamma_2$  we have

$$u(1, y) = \sqrt{2}e^{\gamma y} \sin\left(\frac{\pi(2\beta + 1)}{4}\right),$$

$$\frac{\partial u}{\partial n}(1, y) = \frac{\partial u}{\partial x}(1, y) = \frac{\pi\beta\sqrt{2}}{4}e^{\gamma y} \cos\left(\frac{\pi(2\beta + 1)}{4}\right), \quad y \in (-a, 0),$$

and we can take

$$\alpha(1, y) = -\frac{\beta\pi}{4} \cot\left(\frac{\pi(2\beta + 1)}{4}\right) = \frac{\beta\pi}{4} \tan\left(\frac{\pi(2\beta - 1)}{4}\right), \quad y \in (-a, 0) \quad (2.8)$$

that we can make non-negative by requiring that

$$\beta \in \left[\frac{1}{2}, \frac{3}{2}\right] \cup \left[\frac{5}{2}, \frac{7}{2}\right]. \quad (2.9)$$

Finally, on the horizontal boundary of  $\Gamma_2$  we have

$$u(x, -a) = \sqrt{2}e^{-a\gamma} \sin\left(\frac{\pi}{4}(\beta x + \beta + 1)\right),$$

$$\frac{\partial u}{\partial n}(x, -a) = -\frac{\partial u}{\partial y}(x, -a) = -\gamma\sqrt{2}e^{-a\gamma} \sin\left(\frac{\pi}{4}(\beta x + \beta + 1)\right), \quad x \in (-1, 1),$$

and we can take

$$\alpha(x, -a) = \gamma, \quad x \in (-1, 1) \quad (2.10)$$

that we can make non-negative by taking

$$\gamma = \sqrt{k^2 + \frac{\beta^2\pi^2}{16}}. \quad (2.11)$$

To summarize, one can observe that by taking  $\gamma$  given by (2.11) and  $\beta$  in the intervals given in (2.9), we can satisfy the homogeneous form of the Robin boundary condition (2.2) on  $\Gamma_2$ , independent of the constant positive parameter  $a$ . In addition, the solution (2.5) does not depend on  $a$  and so it will be the Cauchy data (2.1) and (2.3) on  $\Gamma_1 = \{(x, y) \in \mathbb{R}^2 \mid x^2 + y^2 = 1, y \geq 0\}$ . In conclusion,  $a > 0$  cannot be identified from equations (2.1)-(2.3) and (2.6) only, and therefore this is a counterexample to the uniqueness of solution.

We now perform a similar analysis for the Helmholtz equation.

(b) *The Helmholtz equation*

Let us next consider the Helmholtz equation

$$\nabla^2 u + k^2 u = 0 \quad \text{in } \Omega. \quad (2.12)$$

It can be seen that (2.5) satisfies the Helmholtz equation (2.12) if  $\gamma^2 = \beta^2 \pi^2 / 16 - k^2$ , and we immediately require that  $\beta^2 \geq 16k^2 / \pi^2$ . Then on trying to satisfy the homogeneous form of the Robin boundary condition (2.2) on  $\Gamma_2$  as before, one obtains

$$\begin{aligned}\alpha(-1, y) &= \frac{\beta \pi}{4}, \\ \alpha(1, y) &= \frac{\beta \pi}{4} \tan\left(\frac{\pi(2\beta - 1)}{4}\right), \quad y \in (-a, 0), \\ \alpha(x, -a) &= \gamma.\end{aligned}$$

Consequently, if for example we take  $\beta$  to be an odd integer greater or equal than  $4k/\pi$  and  $\gamma = \sqrt{\beta^2 \pi^2 / 16 - k^2}$ , then  $\alpha(1, y) = \beta \pi / 4$  and we satisfy  $\alpha \geq 0$  everywhere on  $\Gamma_2$ . The solution is again not unique, because  $a > 0$  cannot be determined.

### 3. The Method of Fundamental Solutions (MFS)

In the MFS for the Helmholtz (or modified Helmholtz) elliptic equation, we can approximate the solution of equation (1.1) by a linear combination of fundamental solutions with respect to source points placed outside the solution domain — viz.

$$u(\underline{X}) = \sum_{j=1}^N a_j G(\underline{X}, \underline{\xi}^j), \quad \underline{X} \in \overline{\Omega}, \quad (3.1)$$

where the  $N$  vectors  $(\underline{\xi}^j)_{j=1, \overline{N}}$  are distinct source points located outside the domain  $\overline{\Omega}$  and  $G$  is the fundamental solutions of Helmholtz (or modified Helmholtz) equation (1.1). The fundamental solutions of the Helmholtz and the modified Helmholtz in two dimensions are

$$G_H(\underline{X}, \underline{Y}) = H_0^{(1)}(kr) \quad (3.2)$$

and

$$G_{MH}(\underline{X}, \underline{Y}) = K_0(kr) \quad (3.3)$$

respectively, where  $r = \|\underline{X} - \underline{Y}\|$ ,  $i = \sqrt{-1}$  and  $H_0^{(1)} = J_0 + iY_0$  is the Hankel function of the first kind of order zero,  $J_0$  is the Bessel function of the first kind of order zero,  $Y_0$  is the Bessel function of the second kind of order zero, and  $K_0$  is the modified Bessel function of the second kind of order zero. For simplicity, the constants  $i/4$  and  $1/(2\pi)$ , which do not appear in (3.2) and (3.3) respectively, have been embedded in the unknown coefficients  $(a_j)_{j=1, \overline{N}}$  in (3.1). These coefficients are real for the modified Helmholtz equation and complex for the Helmholtz equation. The Bessel functions  $J_0$ ,  $Y_0$  and  $K_0$  can be computed using the NAG routines S17AEF, S17ACF and S18ACE, respectively.

Assume for simplicity that  $\Gamma_1 = \{(r, \theta) \mid r = 1, \theta \in [0, \pi]\}$  is the upper-half of the unit circle, and consider the boundary collocation points

$$\underline{X}_i = (\cos(\tilde{\theta}_i), \sin(\tilde{\theta}_i)), \quad i = \overline{1, M+1}, \quad (3.4)$$

uniformly distributed on the known boundary  $\Gamma_1$  where  $\tilde{\theta}_i = \pi(i-1)/M$  for  $i = \overline{1, M+1}$ . Assume also that the corroded solution domain  $\Omega$  is star-shaped with respect to the origin, such that  $\Gamma_2$  can be parametrised by

$$\Gamma_2 = \{(r(\theta) \cos(\theta), r(\theta) \sin(\theta)) \mid \theta \in (\pi, 2\pi), r(\theta) > 0\}. \quad (3.5)$$

Let

$$\underline{X}_i = (r_{i-M} \cos(\tilde{\theta}_i), r_{i-M} \sin(\tilde{\theta}_i)), \quad i = \overline{M+2, 2M}, \quad (3.6)$$

be boundary collocation points on the unknown boundary  $\Gamma_2$ , where  $r_{i-M} = r(\tilde{\theta}_i)$  and  $\tilde{\theta}_i = \pi(i-1)/M$  for  $i = \overline{M+2, 2M}$ . The source points  $(\underline{\xi}^j)_{j=\overline{1, N}}$  in  $\mathbb{R}^2 \setminus \overline{\Omega}$  are taken to be

$$\underline{\xi}^j = (R \cos(\hat{\theta}_j), R \sin(\hat{\theta}_j)), \quad j = \overline{1, N}, \quad (3.7)$$

where  $R > 1$  and  $\hat{\theta}_j = 2\pi(j-1)/N$  for  $j = \overline{1, N}$ . Typical distributions of the boundary collocation points (3.4) and (3.6), and of the source points (3.7), are schematically shown in Fig. 2.

When  $\alpha$  is known, the MFS coefficient vector  $\underline{a} = (a_j)_{j=\overline{1, N}}$  and the radii vector  $\underline{r} = (r_i)_{i=\overline{2, M}}$  characterising the star-shaped unknown boundary  $\Gamma_2$  can be determined by imposing the boundary conditions (2.1)-(2.3) in a least-squares sense, which recasts into minimising the nonlinear objective function

$$\begin{aligned} T(\underline{a}, \underline{r}) := & \left\| u - f \right\|_{L^2(\Gamma_1)}^2 + \left\| \frac{\partial u}{\partial n} - g \right\|_{L^2(\Gamma_1)}^2 + \left\| \left( \frac{\partial u}{\partial n} + \alpha u \right) - h \right\|_{L^2(\Gamma_2)}^2 \\ & + \lambda_1 \|\underline{a}\|^2 + \lambda_2 \|\underline{r}'\|^2 \end{aligned} \quad (3.8)$$

where  $\lambda_1, \lambda_2 \geq 0$  are regularisation parameters introduced in order to stabilise the numerical solution. The last term in Eq. (3.8) contains a  $C^1$ -smoothing constraint on the sought shape  $\Gamma_2$ . Introducing the MFS approximation (3.1) into Eq. (3.8) yields

$$\begin{aligned} T(\underline{a}, \underline{r}) = & \sum_{i=1}^{M+1} \left| \sum_{j=1}^N a_j G(\underline{X}_i, \underline{\xi}^j) - f(\underline{X}_i) \right|^2 + \sum_{i=M+2}^{2M+2} \left| \sum_{j=1}^N a_j \frac{\partial G}{\partial n}(\underline{X}_{i-M-1}, \underline{\xi}^j) - g(\underline{X}_{i-M-1}) \right|^2 \\ & + \sum_{i=2M+3}^{3M+1} \left| \sum_{j=1}^N a_j \left( \frac{\partial G}{\partial n}(\underline{X}_{i-M-1}, \underline{\xi}^j) + \alpha(\underline{X}_{i-M-1}) G(\underline{X}_{i-M-1}, \underline{\xi}^j) \right) - h(\underline{X}_{i-M-1}) \right|^2 \\ & + \lambda_1 \sum_{j=1}^N |a_j|^2 + \lambda_2 \sum_{j=2}^{M-1} (r_{j+1} - r_j)^2. \end{aligned} \quad (3.9)$$

In the real case, for the modified Helmholtz equation (2.6) the minimisation of (3.9) imposes  $3M+1$  nonlinear equations in the  $N+M-1$  unknowns  $(\underline{a}, \underline{r})$ , so for a unique solution it is necessary that  $2M \geq N-2$ . In the complex case, for the Helmholtz equation (2.12) the minimisation of (3.9) imposes  $6M+2$  nonlinear equations in the  $2N+M-1$  unknowns  $(\underline{a}, \underline{r})$ , so for a unique solution it is necessary that  $5M \geq 2N-3$ .

If there is noise in the measured data (2.3), we replace  $g$  in (3.9) by

$$g^\epsilon(\underline{X}_i) = g(\underline{X}_i) + \epsilon_i, \quad i = \overline{1, M+1}, \quad (3.10)$$

where  $\epsilon_i$  are random variables generated by the NAG routine D05DDF from a Gaussian normal distribution with zero mean and standard deviation

$$\sigma = p \times \max_{\Gamma_1} |g|, \quad (3.11)$$

where  $p$  represents the noise percentage.

In Eq. (3.9), the normal derivatives of the fundamental solution  $G$  obtained via (3.2) and (3.3) are

$$\frac{\partial G_H}{\partial n}(\underline{X}, \underline{\xi}) = -k \frac{(\underline{X} - \underline{\xi}) \cdot \underline{n}}{\|\underline{X} - \underline{\xi}\|} H_1^{(1)}(k\|\underline{X} - \underline{\xi}\|) \quad (3.12)$$

and

$$\frac{\partial G_{MH}}{\partial n}(\underline{X}, \underline{\xi}) = -k \frac{(\underline{X} - \underline{\xi}) \cdot \underline{n}}{\|\underline{X} - \underline{\xi}\|} K_1(k\|\underline{X} - \underline{\xi}\|). \quad (3.13)$$

Here  $H_1^{(1)} = J_1 + iY_1$  is the Hankel function of the first kind of order one,  $J_1$  is the Bessel function of the first kind of order one,  $Y_1$  is the Bessel function of the second kind of order one,  $K_1$  is the modified Bessel function of second kind of order one, and

$$\underline{n}(\underline{X}) = \begin{cases} \cos(\theta)\underline{i} + \sin(\theta)\underline{j}, & \text{if } \underline{X} \in \Gamma_1, \\ \frac{1}{\sqrt{r^2(\theta) + r'^2(\theta)}} \left[ (r'(\theta)\sin(\theta) + r(\theta)\cos(\theta))\underline{i} + (-r'(\theta)\cos(\theta) + r(\theta)\sin(\theta))\underline{j} \right], & \text{if } \underline{X} \in \Gamma_2, \end{cases} \quad (3.14)$$

where  $\underline{i} = (1, 0)$  and  $\underline{j} = (0, 1)$ . The Bessel functions  $J_1$ ,  $Y_1$  and  $K_1$  can be computed using the NAG routines S17AFE, S17ADF and S18ADE, respectively. In Eq. (3.14), the derivative  $r'$  may be approximated using backward finite differences as

$$r'(\tilde{\theta}_{i+M}) \approx \frac{r_i - r_{i-1}}{\pi/M}, \quad i = \overline{2, M}, \quad (3.15)$$

with the convention that  $r_1 = 1$ .

The minimisation of the objective function (3.9) is accomplished computationally using the NAG routine E04FCF, which is a comprehensive algorithm for minimising an unconstrained sum of squares of nonlinear functions. Furthermore, this routine does not require the user to supply the gradient of (3.9), as this is calculated internally using finite differences. If required, the constraints  $r_i > 0$  for  $i = \overline{2, M}$  can be imposed manually during the iterative procedure by adjustment at each iteration. The minimisation process usually terminates when either a user-specified tolerance is achieved, or when a user-specified

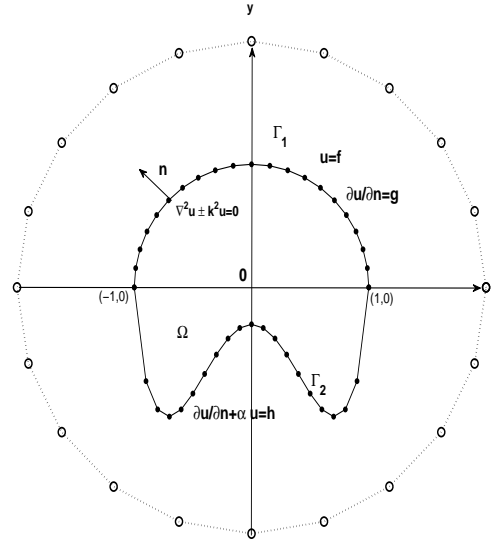


Figure 2: Typical distribution of source (o) and boundary collocation (•) points.

maximum number of iterations is reached.

Finally, we observe that the form of the functional (3.8) contains a single measurement of the Neumann flux  $g$  for prescribed Dirichlet boundary data  $f$ , via the operational relation (2.3). However, in some cases, one may need to use two measured fluxes  $g_1$  and  $g_2$  for two prescribed linearly independent boundary data  $f_1$  and  $f_2$ , via the operational relation (2.3). This means that we double up the number of equations in (3.8), which now reads

$$\begin{aligned}
 T(\underline{a}^{(1)}, \underline{a}^{(2)}, \underline{r}) := & \left\| u_1 - f_1 \right\|_{L^2(\Gamma_1)}^2 + \left\| u_2 - f_2 \right\|_{L^2(\Gamma_1)}^2 + \left\| \frac{\partial u_1}{\partial n} - g_1 \right\|_{L^2(\Gamma_1)}^2 + \left\| \frac{\partial u_2}{\partial n} - g_2 \right\|_{L^2(\Gamma_1)}^2 \\
 & + \left\| \left( \frac{\partial u_1}{\partial n} + \alpha u_1 \right) - h \right\|_{L^2(\Gamma_2)}^2 + \left\| \left( \frac{\partial u_2}{\partial n} + \alpha u_2 \right) - h \right\|_{L^2(\Gamma_2)}^2 \\
 & + \lambda_1 \left( \left\| \underline{a}^{(1)} \right\|^2 + \left\| \underline{a}^{(2)} \right\|^2 \right) + \lambda_2 \left\| \underline{r}' \right\|^2, \tag{3.16}
 \end{aligned}$$

where  $\underline{a}^{(1)}$  and  $\underline{a}^{(2)}$  are the corresponding unknown coefficients in the MFS expansion (3.1) for approximating the solutions of the inverse problems with the Dirichlet data  $f_1$  and  $f_2$ , respectively.

#### 4. Numerical Results and Discussion

Numerical results are now presented for  $R = 2$  for Examples 4.1 and 4.2, and for  $R = 3$  for Examples 4.3 – 4.5, with  $M = 14$  and  $N = 28$ . The use of higher MFS parameters  $M$

and  $N$  did not affect significantly the accuracy of the numerical results, but it may become prohibitive. Moreover, the initial guess for the vector  $\underline{a}$  is  $\underline{1.0}$ , and the initial guess for the unknown part of the boundary  $\Gamma_2$  is taken as the lower-half of the circle located at the origin with radius 0.5. In all numerical experiments, as required by the NAG routine E04FCF used, the tolerance  $X\text{Tol}$  was set to  $10^{-6}$ , and the maximum number of function evaluations  $\text{MAXCAL}$  was set to  $400(N + M - 1)$  for the first four examples and to  $800(N + M - 1)$  for the fifth example. In all examples, the corroded boundary  $\Gamma_2$  is unknown. Also, in the first four examples the Robin coefficient  $\alpha$  is known, whilst in the fifth example  $\alpha$  is unknown. In comparison with the numerical MFS investigations concerning sound-soft (Dirichlet boundary condition applies on  $\Gamma_2$ ) or sound-hard (Neumann boundary condition applies on  $\Gamma_2$ ) boundary identification of Ref. [23], the novelty here is solving different inverse problems to determine an unknown absorbing boundary  $\Gamma_2$  on which the Robin boundary condition (2.2) applies. In addition, the Robin surface coefficient  $\alpha$  can also be considered unknown — cf. Example 4.5. For the Helmholtz equation (2.12), the main difficulty in solving either the direct or inverse problem is the case when  $k$  is large. Nevertheless, there are studies (e.g. [8]) that deal with this high frequency case, but this issue will not be pursued here. Indeed, for simplicity we only illustrate numerical results for the modified Helmholtz equation (2.6) free of any such difficulty for large wavenumbers.

**Example 4.1.** We consider the unit disc domain  $\Omega = \{(x, y) \in \mathbb{R}^2 \mid x^2 + y^2 < r = 1\}$ , with boundary divided into two parts — viz.

$$\Gamma_1 = \{(x, y) \in \mathbb{R}^2 \mid x = \cos(\theta); y = \sin(\theta); \theta \in [0, \pi]\} \quad (4.1)$$

and

$$\Gamma_2 = \{(x, y) \in \mathbb{R}^2 \mid x = r(\theta) \cos(\theta); y = r(\theta) \sin(\theta); \theta \in (\pi, 2\pi), r(\theta) = 1\}. \quad (4.2)$$

We take the Dirichlet data (2.1) on  $\Gamma_1$  given by

$$u(1, \theta) = f(\theta) = e^{\cos(\theta) + \sin(\theta)}, \quad \theta \in [0, \pi], \quad (4.3)$$

the Neumann data (2.3) on  $\Gamma_1$  given by

$$\frac{\partial u}{\partial n}(1, \theta) = g(\theta) = (\cos(\theta) + \sin(\theta))e^{\cos(\theta) + \sin(\theta)}, \quad \theta \in [0, \pi], \quad (4.4)$$

and the inhomogeneous Robin boundary condition (2.2) on  $\Gamma_2$  given by

$$\frac{\partial u}{\partial n}(r(\theta), \theta) + \alpha(\theta)u(r(\theta), \theta) = h(\theta) = (\cos(\theta) + \sin(\theta) + \alpha(\theta))e^{\cos(\theta) + \sin(\theta)}, \quad \theta \in (\pi, 2\pi), \quad (4.5)$$

where  $\alpha(\theta)$  is a given non-negative function.

In Example 4.1, assuming that  $\alpha$  is known the analytical solution for the modified Helmholtz equation (2.6) for  $k = \sqrt{2}$  satisfying (4.3)-(4.5) is given by

$$u(x, y) = e^{x+y}, \quad (x, y) \in \overline{\Omega}, \quad (4.6)$$

and  $\Gamma_2$  given by expression (4.2).

**Example 4.2.** We also consider a more complicated geometric shape with boundary divided into two parts — viz.  $\Gamma_1$  is the upper-half of the circle given by expression (4.1), and  $\Gamma_2$  is the lower-half of a peanut shape parametrised by

$$\Gamma_2 = \left\{ (x, y) \in \mathbb{R}^2 \mid x = r(\theta) \cos(\theta); y = r(\theta) \sin(\theta); \theta \in (\pi, 2\pi), \right. \\ \left. r(\theta) = \sqrt{\cos^2(\theta) + \frac{1}{4} \sin^2(\theta)} \right\}. \quad (4.7)$$

The Dirichlet data (2.1) on  $\Gamma_1$  is given by (4.3), the Neumann data (2.3) on  $\Gamma_1$  is given by (4.4) and the inhomogeneous Robin boundary condition on  $\Gamma_2$  is given by

$$\frac{\partial u}{\partial n}(r(\theta), \theta) + \alpha(\theta)u(r(\theta), \theta) = h(\theta) = e^{r(\theta)(\cos(\theta)+\sin(\theta))} \left( \alpha(\theta) + (1, 1) \cdot \underline{n}(\theta) \right), \\ \theta \in (\pi, 2\pi), \quad (4.8)$$

where  $\underline{n}$  is given by the second branch of expression (3.14),  $r(\theta)$  is given by (4.7) and  $r'(\theta) = -3 \sin(2\theta)/(8r(\theta))$ . Assuming that  $\alpha$  is known, the analytical solution for the modified Helmholtz equation (2.6) for  $k = \sqrt{2}$  satisfying (4.3), (4.4) and (4.8) is given by (4.6) and  $\Gamma_2$  is given by expression (4.7).

**(a) Case I (Dirichlet boundary condition)**

We first consider the case when the Dirichlet boundary condition applies on  $\Gamma_2$ , such that the first term in equation (2.2) is ignored ( $\partial u / \partial n = 0$  and we take  $\alpha = 1$ ). Thus we consider the Dirichlet boundary condition on  $\Gamma_2$  given by

$$u(1, \theta) = h(\theta) = e^{\cos(\theta)+\sin(\theta)}, \quad \theta \in (\pi, 2\pi). \quad (4.9)$$

**No noise.** We now consider the case when there is no noise (i.e.  $p = 0$ ) in the input flux data (4.4). Figs. 3(a) and 4(a) show the objective function (3.9) without regularisation — i.e.  $\lambda_1 = \lambda_2 = 0$  as a function of the number of iterations, for Examples 4.1 and 4.2 respectively. It can be seen that the objective function decreases rapidly to a very low stationary level  $\mathbf{O}(10^{-15})$ , in about 26 and 31 iterations respectively. The corresponding exact and reconstructed shapes of the boundary  $\Gamma_2$  are presented in Figs. 3(b) and 4(b). From these figures, it can clearly be seen that the numerically reconstructed shapes are stable and accurate in comparison with the exact shapes (4.2) and (4.7).

**Adding noise.** We consider now the case when there is  $p = \{1\%, 3\%, 5\%$  noise in the input flux data (4.4), added as in (3.10). Although not illustrated, the numerical results

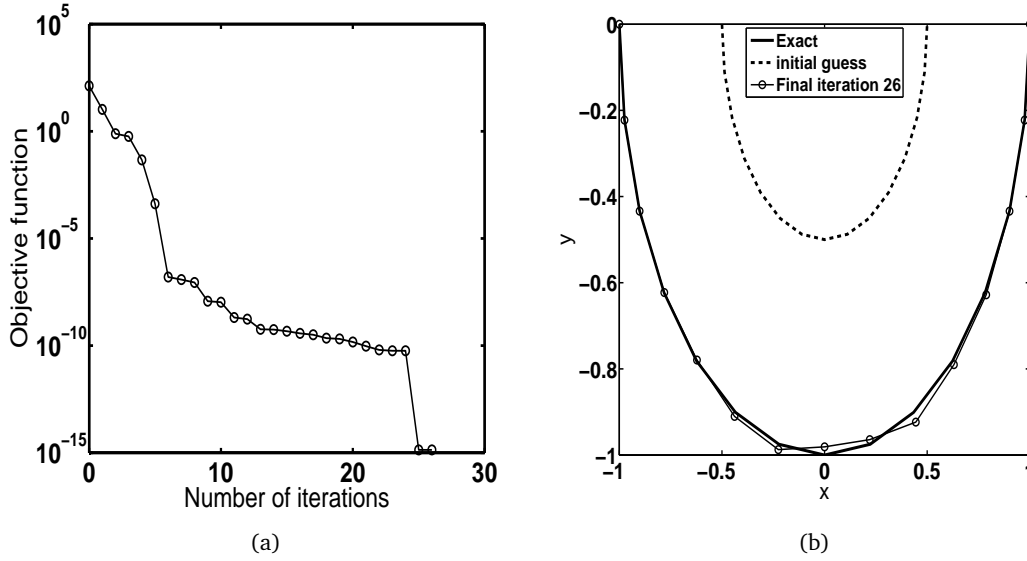


Figure 3: (a) The objective function and (b) Initial guess, exact and numerically reconstructed shapes of the boundary  $\Gamma_2$  for Example 4.1, *Case I* when there is no noise in the data (4.4) and no regularisation.

with no regularisation imposed in the nonlinear least-squares functional (3.9) were found to be unstable and highly inaccurate. This is to be expected, since the inverse problem under investigation is ill-posed and therefore regularisation is needed in order to obtain stable solutions.

Figs. 5 and 6 show the regularised objective function and the retrieved boundary  $\Gamma_2$ , obtained with the regularisation parameters  $\lambda_1 = 10^{-5}, \lambda_2 = 10^{-1}$  for Example 4.1 and  $\lambda_1 = \lambda_2 = 10^{-2}$  for Example 4.2. From the computational experiments, it is notable that if the regularisation parameters  $\lambda_1$  and  $\lambda_2$  are too small then oscillating unstable solutions are obtained. However, from Figs. 5(b) and 6(b) it is seen that reasonably stable numerical solutions can be obtained if the regularisation parameters  $\lambda_1$  and  $\lambda_2$  are properly tuned. In our work, we chose these parameters by trial and error, although one can also try the L-surface framework proposed by Belge *et al.* [3]. From these figures, it can also be seen that the numerical solutions become more accurate as the amount of noise  $p$  in the input data decreases.

**(b) Case II (Neumann boundary condition)**

We consider a second case when the Neumann boundary condition ( $\alpha = 0$ ) applies on  $\Gamma_2$ , such that the second term in equation (2.2) is ignored ( $au = 0$ ). Thus we consider the Neumann boundary condition on  $\Gamma_2$  given by

$$\frac{\partial u}{\partial n}(1, \theta) = h(\theta) = (\cos(\theta) + \sin(\theta)) e^{\cos(\theta) + \sin(\theta)}, \quad \theta \in (\pi, 2\pi). \quad (4.10)$$

The numerical results for Example 4.1 obtained for *Case II*, illustrated in Figs. 7 and 8, are similar to those obtained in Figs. 3 and 5 for *Case I*. We finally report that the accuracy and

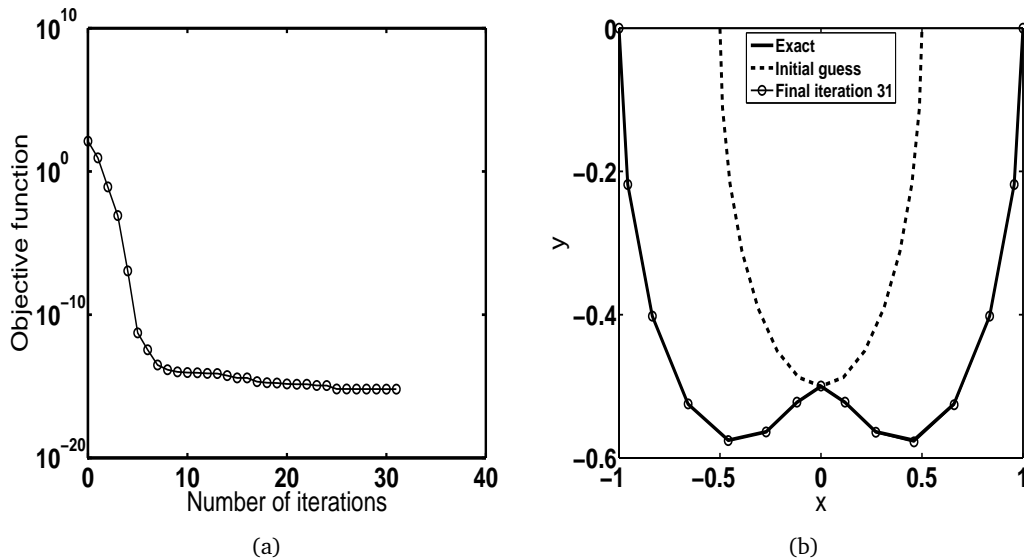


Figure 4: (a) The objective function and (b) Initial guess, exact and numerically reconstructed shapes of the boundary  $\Gamma_2$  for Example 4.2, Case I when there is no noise in the data (4.4) and no regularisation.

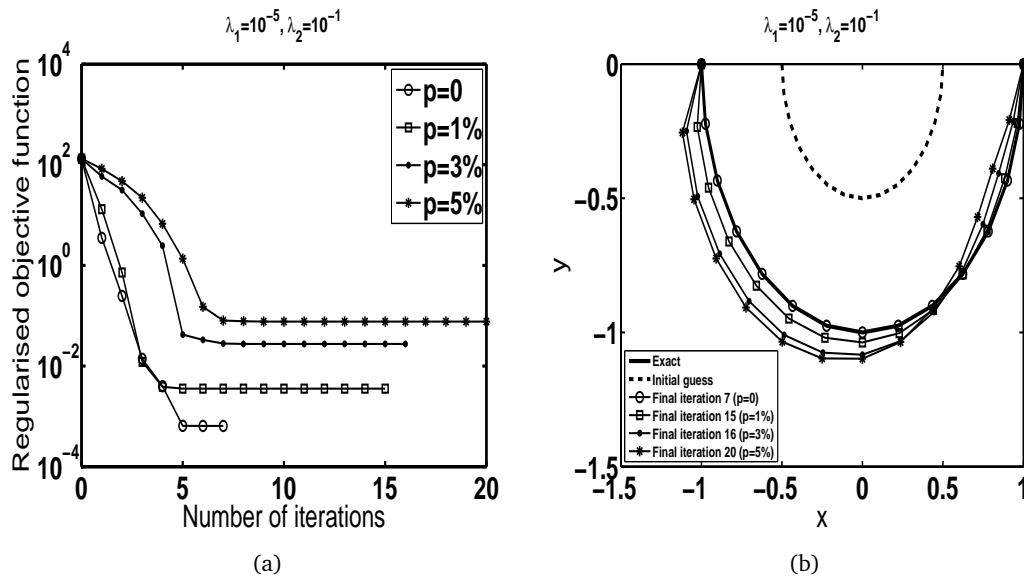


Figure 5: (a) The regularised objective function and (b) Initial guess, exact and numerically reconstructed shapes of the boundary  $\Gamma_2$  for Example 4.1, Case I when there is  $p = \{0, 1\%, 3\%, 5\%\}$  noise in the data (4.4) and  $\lambda_1 = 10^{-5}, \lambda_2 = 10^{-1}$ .

stability numerical results presented in Figs. 3-8 for the Cases I and II are similar to those obtained in Ref. [23]. However, in that reference a different NAG routine was used and some computational details are different.

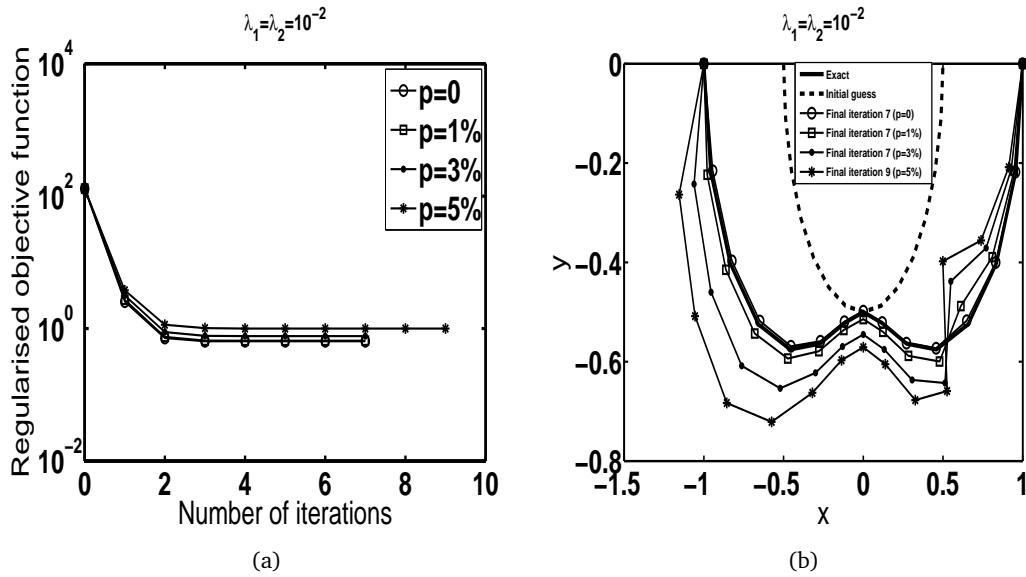


Figure 6: (a) The regularised objective function and (b) Initial guess, exact and numerically reconstructed shapes of the boundary  $\Gamma_2$  for Example 4.2, Case I when there is  $p = \{0, 1\%, 3\%, 5\%$  noise in the data (4.4) and  $\lambda_1 = \lambda_2 = 10^{-2}$ .

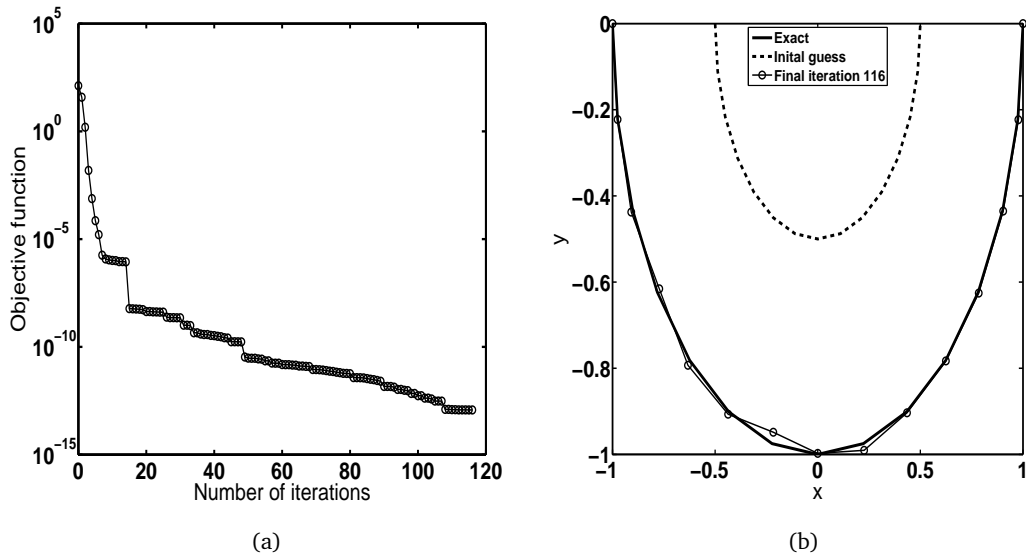


Figure 7: (a) The objective function and (b) Initial guess, exact and numerically reconstructed shapes of the boundary  $\Gamma_2$  for Example 4.1, Case II when there is no noise in the data (4.4) and no regularisation.

In the remainder of this section, the numerical investigation departs from the analysis of Ref. [23]. For the sake of our preliminary investigation into an ill-posed problem, which may lack a unique solution (cf. the discussion in Section 2), we consider only the determi-

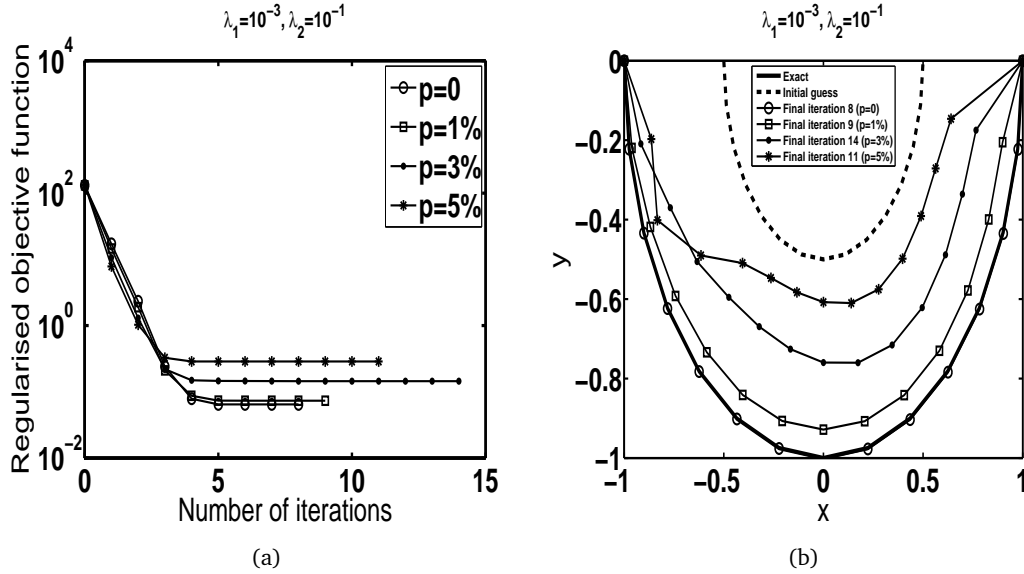


Figure 8: (a) The regularised objective function and (b) Initial guess, exact and numerically reconstructed shapes of the boundary  $\Gamma_2$  for Example 4.1, *Case II* when there is  $p = \{0, 1\%, 3\%, 5\%\}$  noise in the data (4.4) and  $\lambda_1 = 10^{-3}$ ,  $\lambda_2 = 10^{-1}$ .

nation of the semicircular boundary (4.2). The retrieval of more complicated shapes, such as the lower-half of the peanut shape (4.7) under the Robin boundary condition (2.2), is deferred to a future investigation.

### (c) Case III (Robin boundary condition)

The third case involves the Robin boundary condition (4.5) with  $\alpha = 1$  applied on  $\Gamma_2$ . Unlike in Figs. 3 and 7 for the previous Dirichlet and Neumann cases (*Cases I and II*), Fig. 9 shows that in the Robin *Case III* the numerical results appear unstable even for exact data ( $p = 0$ ) if no regularisation is imposed on (3.9). Indeed, a slight amount of regularisation is needed in order to obtain stable solutions and the stable and accurate numerical results also illustrated in Fig. 9. For noisy data, the numerical results obtained for *Case III* in Fig. 10 are similar to those obtained in Fig. 5 for *Case I* and in Fig. 8 for *Case II*.

In the previous two examples we have considered non-homogeneous boundary conditions (4.5) or (4.8) on the unknown corroded boundary  $\Gamma_2$ . In the next examples, we consider the more physical homogeneous Robin boundary condition — i.e.  $h = 0$  in Eq. (2.2) on  $\Gamma_2$ .

**Example 4.3.** The unit disk domain  $\Omega = B(\mathbf{0}; 1)$  is considered as in Example 4.1, and the boundary is divided into two parts as in (4.1) and (4.2). We take the Dirichlet data (2.1) on  $\Gamma_1$  given by

$$u(1, \theta) = f(\theta) = \sqrt{2}e^{\gamma \sin(\theta)} \sin\left(\frac{\pi}{4}(\beta \cos(\theta) + \beta + 1)\right), \quad \theta \in [0, \pi], \quad (4.11)$$

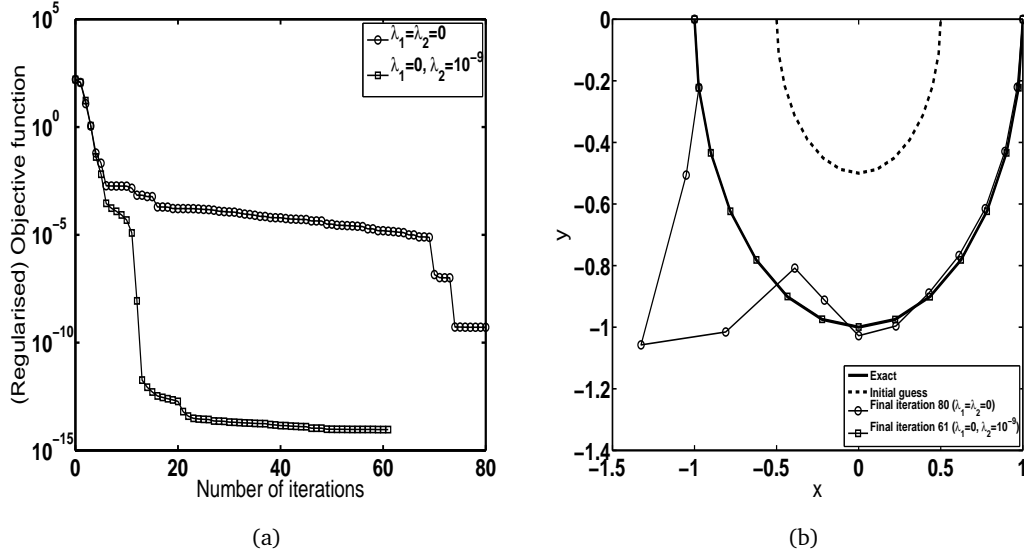


Figure 9: (a) The objective and regularised objective functions and (b) Initial guess, exact and numerically reconstructed shapes of the boundary  $\Gamma_2$  for Example 4.1, Case III when there is no noise in the data (4.4), and with regularisation  $\lambda_1 = 0, \lambda_2 = 10^{-9}$  and without regularisation  $\lambda_1 = \lambda_2 = 0$ .

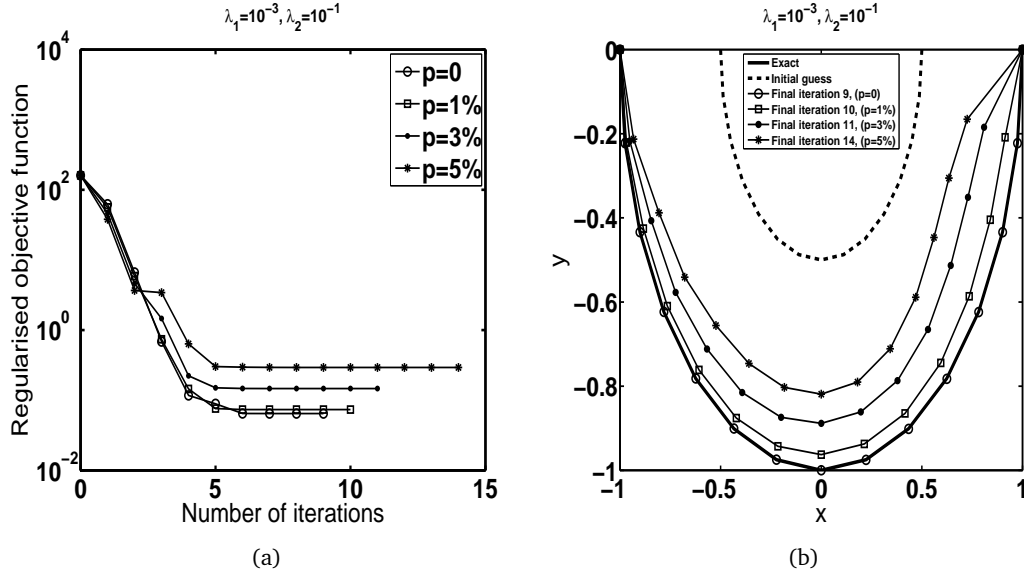


Figure 10: (a) The regularised objective function and (b) Initial guess, exact and numerically reconstructed shapes of the boundary  $\Gamma_2$  for Example 4.1, Case III when there is  $p = \{0, 1\%, 3\%, 5\%\}$  noise in the data (4.4) and  $\lambda_1 = 10^{-3}, \lambda_2 = 10^{-1}$ .

where  $\gamma = \sqrt{\beta^2 \pi^2 / 16 + k^2}$  and the Neumann data (2.3) on  $\Gamma_1$  given by

$$\begin{aligned} \frac{\partial u}{\partial n}(1, \theta) = \frac{\partial u}{\partial r}(1, \theta) = g(\theta) = \sqrt{2} e^{\gamma \sin(\theta)} \left[ \gamma \sin(\theta) \sin\left(\frac{\pi}{4}(\beta \cos(\theta) + \beta + 1)\right) \right. \\ \left. + \frac{\beta \pi \cos(\theta)}{4} \cos\left(\frac{\pi}{4}(\beta \cos(\theta) + \beta + 1)\right) \right], \quad \theta \in [0, \pi]. \end{aligned} \quad (4.12)$$

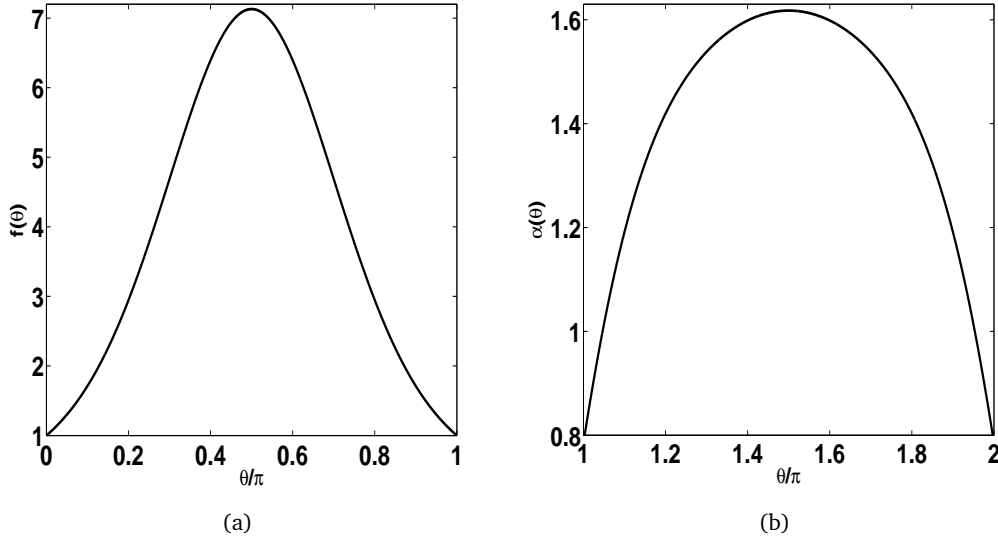


Figure 11: (a) The Dirichlet boundary data (4.11); and (b) the Robin coefficient (4.14) for  $\beta = 1$ ,  $k = \sqrt{2}$ ,  $\gamma = \sqrt{\pi^2/16 + 2}$ .

We also take the homogeneous Robin boundary condition (2.2) on  $\Gamma_2$  (i.e.  $h \equiv 0$ ),

$$\frac{\partial u}{\partial n}(1, \theta) + \alpha(\theta)u(1, \theta) = 0, \quad \theta \in (\pi, 2\pi), \quad (4.13)$$

where  $\alpha$  is the positive Robin coefficient given by

$$\alpha(\theta) = -\gamma \sin(\theta) - \frac{\beta\pi}{4} \cos(\theta) \cot\left(\frac{\pi}{4} (\beta \cos(\theta) + \beta + 1)\right), \quad \theta \in (\pi, 2\pi). \quad (4.14)$$

Graphs of the Dirichlet data (4.11) and the Robin coefficient (4.14) for  $\beta = 1$ ,  $k = \sqrt{2}$  and  $\gamma = \sqrt{\pi^2/16 + 2}$  are presented in Figs. 11(a) and 11(b) respectively, showing that they are positive.

In this example, assuming that  $\alpha$  is known and given by expression (4.14), the analytical solution for the modified Helmholtz equation (2.6) satisfying (4.11)-(4.14) is given by equation (2.5) and  $\Gamma_2$  is given by expression (4.2). As in Example 4.1, the numerical results obtained using regularisation with and without noise in the input data (4.12) illustrated in Figs. 12 and 13 show that the numerical solutions are accurate and stable.

For all the examples considered so far an analytical solution is available, but not in the next example.

**Example 4.4.** Here we change the Dirichlet data (4.11) on  $\Gamma_1$  to

$$u(1, \theta) = f(\theta) = \sin(\theta) - \sin^2(\theta), \quad \theta \in [0, \pi], \quad (4.15)$$

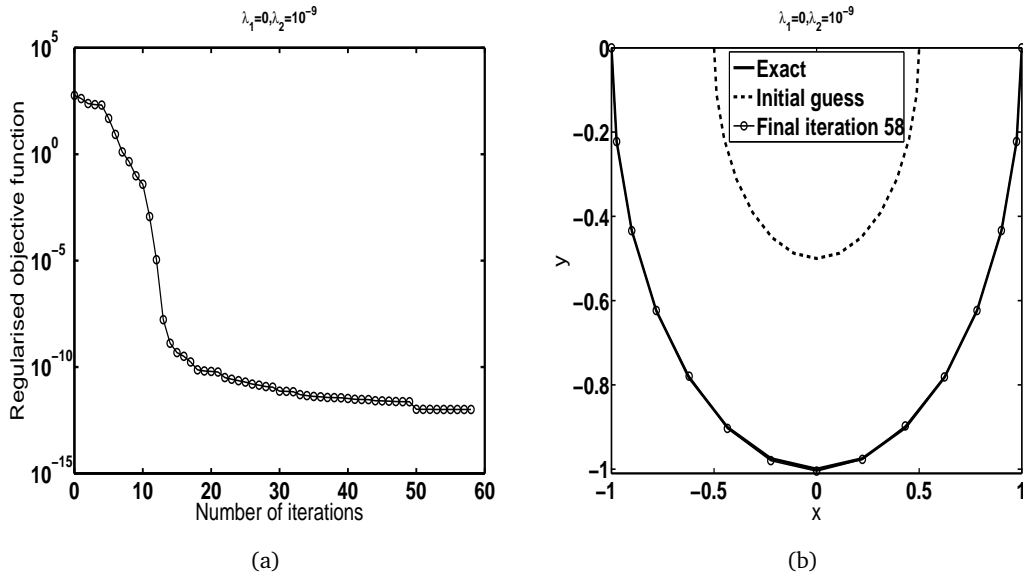


Figure 12: (a) The regularised objective function; and (b) Initial guess, exact and numerically reconstructed shapes of the boundary  $\Gamma_2$  for Example 4.3, when there is no noise in the data (4.12) and  $\lambda_1 = 0, \lambda_2 = 10^{-9}$ .

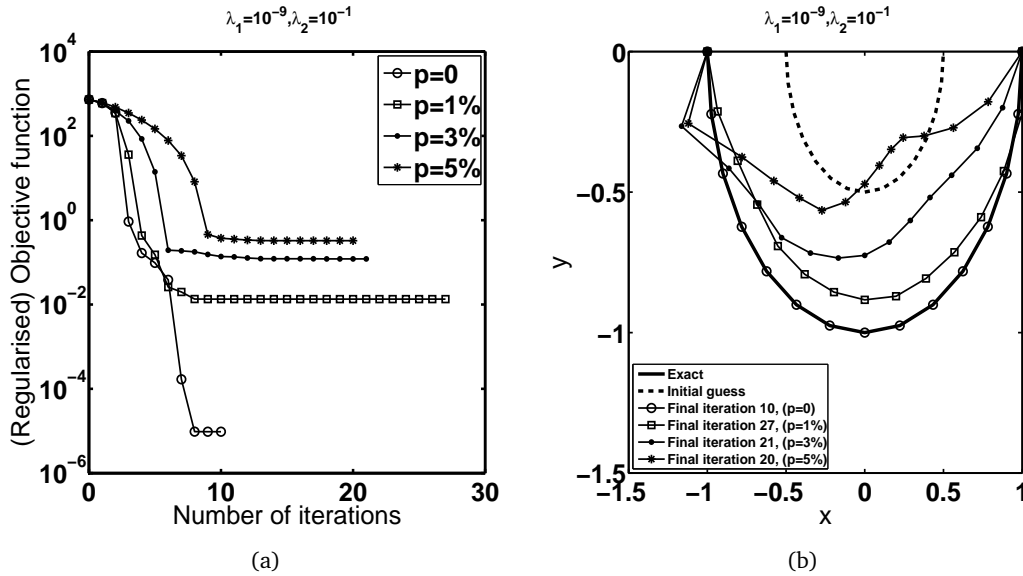


Figure 13: (a) The regularised objective function; and (b) Initial guess, exact and numerically reconstructed shapes of the boundary  $\Gamma_2$  for Example 4.3, when there is  $p = \{0, 1\%, 3\%, 5\%$  noise in the data (4.12) and  $\lambda_1 = 10^{-9}, \lambda_2 = 10^{-1}$ .

but we keep the same homogeneous Robin boundary condition (4.13) with the Robin coefficient given by (4.14) and  $\beta = 1, k = \sqrt{2}, \gamma = \sqrt{\pi^2/16 + 2}$ .

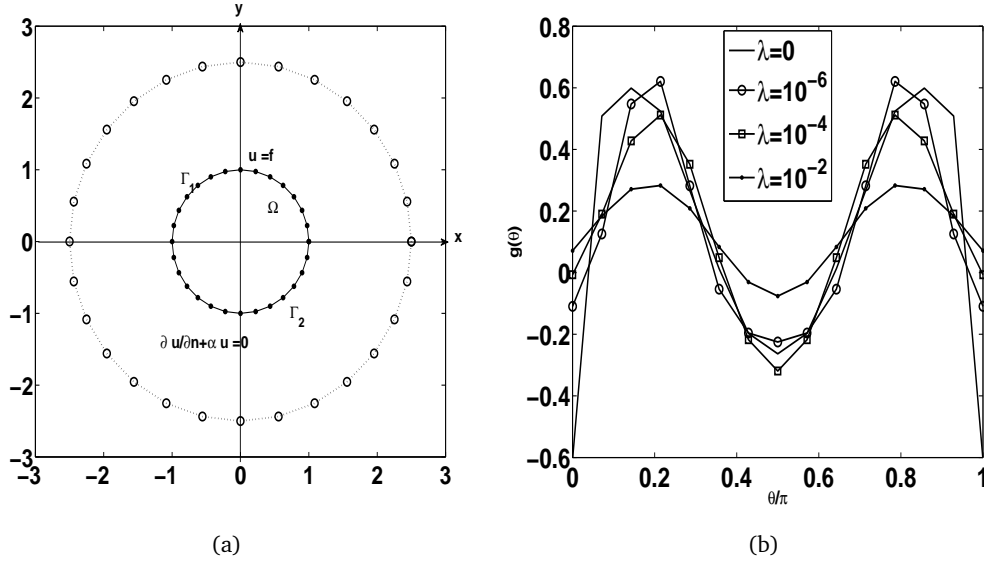


Figure 14: (a) Distribution of source ( $\circ$ ) and boundary collocation ( $\bullet$ ) points; and (b) the numerical solutions for the normal derivative  $g(\theta)$  obtained by solving the direct mixed problem with various regularisation parameters  $\lambda \in \{0, 10^{-6}, 10^{-4}, 10^{-2}\}$ , for Example 4.4.

### Direct Problem

Since in this case no analytical solution is available, the Neumann data (2.3) on  $\Gamma_1$  is simulated numerically by using the MFS to solve the direct mixed problem given by the modified Helmholtz equation (2.6), the homogeneous Robin boundary condition (4.13) on  $\Gamma_2$ , and the Dirichlet boundary condition (4.15) on  $\Gamma_1$ , when  $\Gamma_2$  is known and given by the semi-circle (4.2). The arrangement of the source and boundary collocation points are shown in Fig. 14(a). The numerical solutions for the normal derivative  $g(\theta) = \partial u/\partial n(1, \theta)$  on  $\Gamma_1$ , obtained with  $R = 2.5$  for various regularisation parameters  $\lambda \in \{0, 10^{-6}, 10^{-4}, 10^{-2}\}$  and  $M = 14, N = 28$  are shown in Fig. 14(b). The curve obtained for  $\lambda = 10^{-4}$  in Fig. 14(b) is chosen as the most accurate representation of the unavailable exact solution, because it at least satisfies the continuity of the flux at the end points  $x = \pm 1$  where the Dirichlet and Robin boundary conditions meet. Indeed, from (4.15) we have that  $u(1, 0) = u(1, \pi) = 0$ , and the homogeneous Robin condition (4.13) then also yields  $\partial u/\partial r(1, 0) = \partial u/\partial r(1, \pi) = 0$ . Next, this curve corresponding to  $\lambda = 10^{-4}$  in Fig. 14(b) is used as the input flux data (2.3) in the inverse problem.

### Inverse Problem

Assuming now that  $\Gamma_2$  is unknown, in order to avoid committing an inverse crime the inverse MFS is applied with a different  $R$  than 2.5, say  $R = 3$ . The input Neumann data (2.3) is chosen from the curve  $\lambda = 10^{-4}$  of Fig. 14(b), the Dirichlet data (2.2) is given by (4.15), and the homogeneous Robin boundary condition (4.13) on  $\Gamma_2$  is considered.

The numerical results illustrated in Fig. 15, obtained using regularisation with and

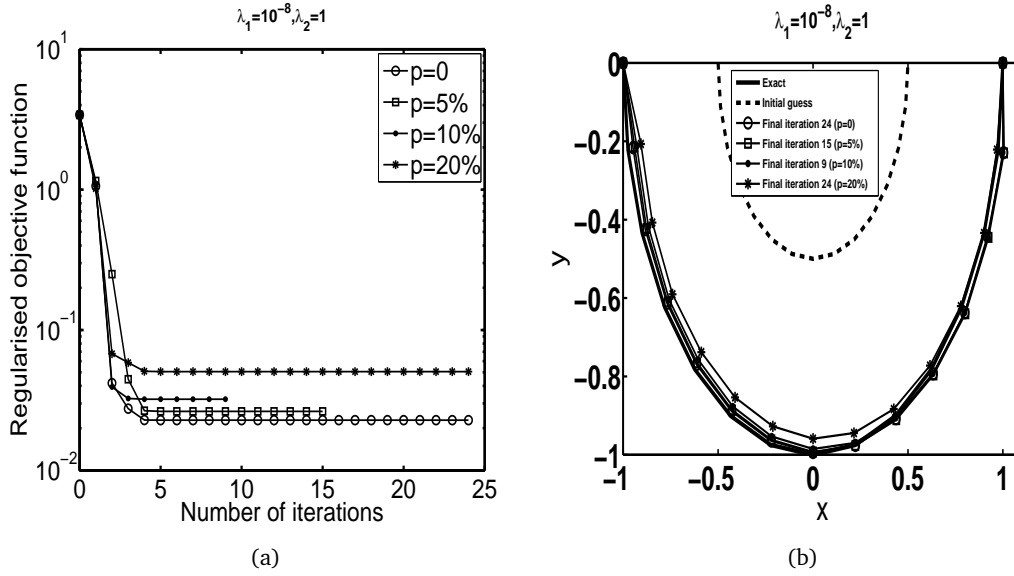


Figure 15: (a) The regularised objective function and (b) Initial guess, exact and numerically reconstructed shapes of the boundary  $\Gamma_2$  for Example 4.4, when there is  $p = \{0, 1\%, 3\%, 5\%$  noise in the data (2.3) and  $\lambda_1 = 10^{-8}, \lambda_2 = 1$ .

without noise in the input data, show that the numerical solutions are accurate and stable even for a large amount of noise (up to  $p = 20\%$ ).

The examples analysed so far considered the inverse problem where the Robin coefficient  $\alpha$  was assumed known. The next and final example considers the case when this coefficient is unknown.

**Example 4.5.** We assume now that both  $\Gamma_2$  and  $\alpha$  are unknown. In order to ensure a unique solution, we combine the Dirichlet data (4.11) and (4.15) on  $\Gamma_1$  as

$$\begin{aligned} u_1(1, \theta) = f_1(\theta) &= \sqrt{2}e^{\gamma \sin(\theta)} \sin\left(\frac{\pi}{4}(\beta \cos(\theta) + \beta + 1)\right), \\ u_2(1, \theta) = f_2(\theta) &= \sin(\theta) - \sin^2(\theta), \quad \theta \in [0, \pi], \end{aligned} \quad (4.16)$$

with  $k = \sqrt{2}$ ,  $\beta = 1$ ,  $\gamma = \sqrt{\pi^2/16 + 2}$ . These Dirichlet boundary data are linearly independent with at least one positive (cf. Fig. 11(a)), and they induce the fluxes  $g_1$  and  $g_2$  via the operational relation (2.3). Since the Robin coefficient  $\alpha$  is now also unknown — i.e. the functional  $T$  appearing in the left-hand side of (3.16) also depends on  $\alpha$ , as  $T(\underline{a}^{(1)}, \underline{a}^{(2)}, \underline{r}, \underline{\alpha})$  — we add in either the zeroth-order regularisation term  $\lambda_3 \|\underline{\alpha}\|^2$  or the first-order regularisation term  $\lambda_3 \|\underline{\alpha}'\|^2$ . We also add noise in the flux  $g_2$ . The numerical results obtained for various amounts of noise are shown in Figs. 16-18, where it can be seen that the numerical solutions are stable with respect to the noise included in the input data. Moreover, the first-order regularisation in  $\alpha$  improves the accuracy of the results over the zeroth-order regularisation. Finally, we remark that the reconstruction of the

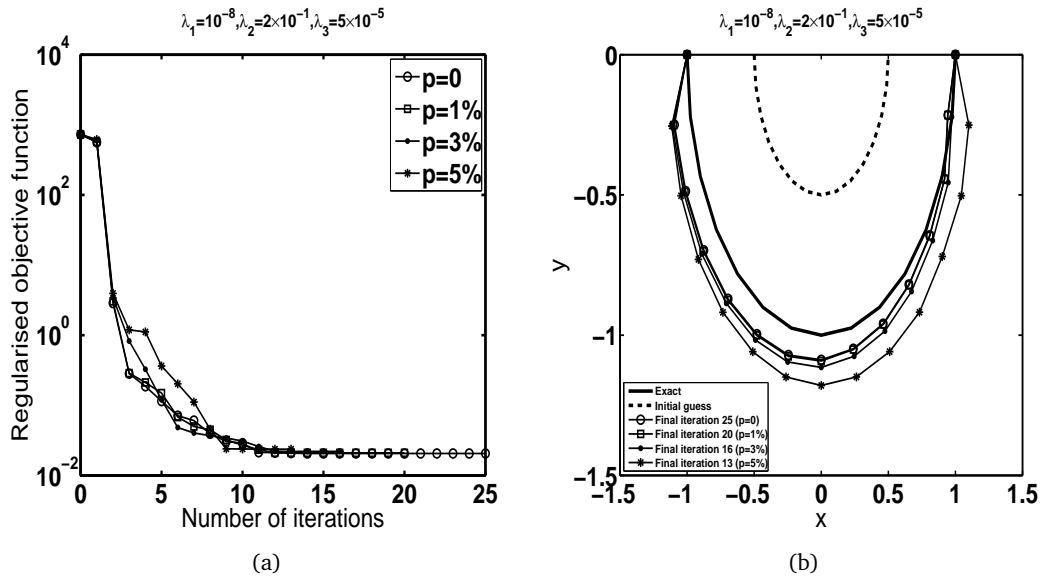


Figure 16: (a) The regularised objective function; and (b) Initial guess, exact and numerically zeroth-order regularisation (in  $\alpha$ ) reconstructed shapes of the boundary  $\Gamma_2$  for Example 4.5, when there is  $p = \{0, 1\%, 3\%, 5\%$  noise in the data (2.3) and  $\lambda_1 = 10^{-8}$ ,  $\lambda_2 = 2 \times 10^{-1}$ ,  $\lambda_3 = 5 \times 10^{-5}$ .

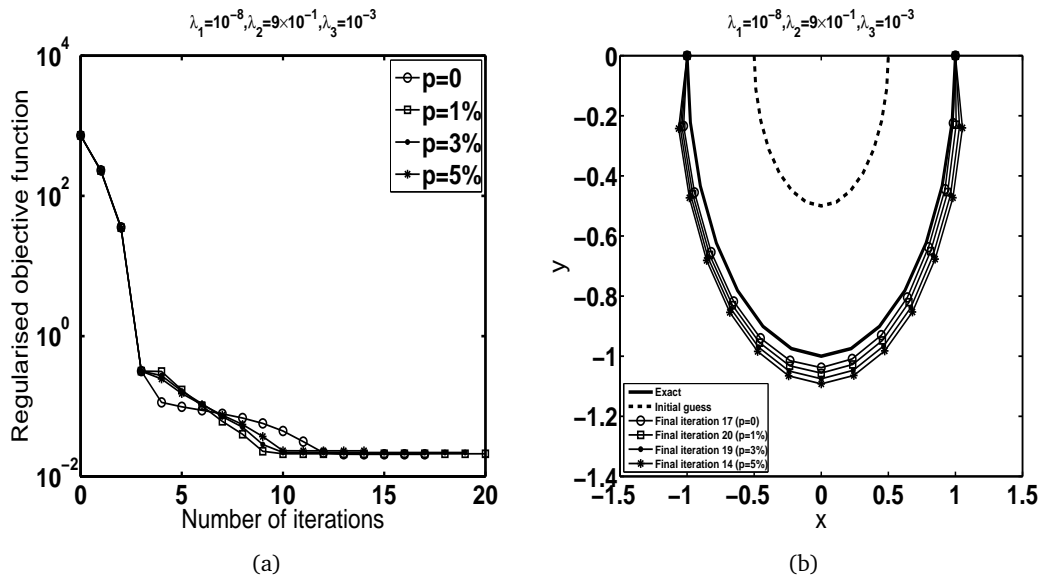


Figure 17: (a) The regularised objective function; and (b) Initial guess, exact and numerically first-order regularisation (in  $\alpha$ ) reconstructed shapes of the boundary  $\Gamma_2$  for Example 4.5, when there is  $p = \{0, 1\%, 3\%, 5\%$  noise in the data (2.3) and  $\lambda_1 = 10^{-8}$ ,  $\lambda_2 = 9 \times 10^{-1}$ ,  $\lambda_3 = 10^{-3}$ .

Robin coefficient  $\alpha$  proves more difficult than the reconstruction of the corroded boundary  $\Gamma_2$ .

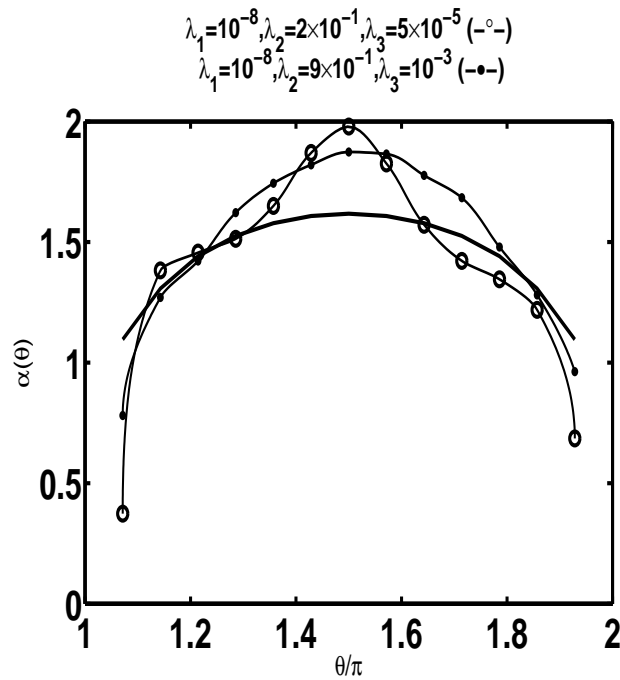


Figure 18: The numerical zeroth-order (-o-), first-order (-.-) and exact (—) solutions for the Robin coefficient  $\alpha$  for Example 4.5, when there is no noise in the data (2.3).

### 5. Conclusions

Two-dimensional Helmholtz-type inverse geometric problems, which involve determining an unknown portion of the boundary  $\Gamma_2$  and its Robin coefficient from one or two linearly independent pairs of Cauchy data on the known boundary  $\Gamma_1 = \partial\Omega \setminus \Gamma_2$ , have been investigated using the MFS. More precisely, a nonlinear regularized MFS is used, in order to obtain stable and accurate numerical results for the ill-posed inverse problem in question. Several examples have been investigated, showing that the numerical results are satisfactory reconstructions for the corroded boundary and its Robin coefficient, with reasonable stability against noisy data.

Future work will consider extending the numerical method developed in this study to solve for the shape and impedance in inverse scattering, governed by the Helmholtz equation in exterior unbounded domains [9, 16, 30].

### Acknowledgments

B. Bin-Mohsin would like to thank King Saud University for their financial support in this research. The comments and suggestions made by the referee are gratefully acknowledged.

## References

- [1] M.T. Ahmed, J.D. Lavers and P.E. Burke (1989) *An evaluation of the direct boundary element method and the method fundamental solutions*, IEEE Trans. Magn., **25**, 3001-3006.
- [2] V. Bacchelli (2009) *Uniqueness for the determination of unknown boundary and impedance with homogeneous Robin condition*, Inverse Problems, **25**, 015004 (4pp).
- [3] M. Belge, M.E. Kilmer and E.L. Miller (2002) *Efficient determination of multiple regularization parameters in a generalized L-curve framework*, Inverse Problems, **18**, 1161-1183.
- [4] E. Cabib, D. Fasino and E. Sincich (2011) *Linearization of a free boundary problem in corrosion detection*, J. Math. Anal. Appl., **378**, 700-709.
- [5] F. Cakoni and R. Kress (2007) *Integral equations for inverse problems in corrosion detection from partial Cauchy data*, Inverse Problems and Imaging, **1**, 229-245.
- [6] F. Cakoni, R. Kress and C. Schuft (2010) *Integral equations for shape and impedance reconstruction in corrosion detection*, Inverse Problems, **26**, 095012 (24pp).
- [7] S. Chaabane and M. Jaoua (1999) *Identification of Robin coefficients by means of boundary measurements*, Inverse Problems, **15**, 1425-1438.
- [8] S.N. Chandler-Wilde, S. Langdon and L. Ritter (2004) *A high-wavenumber boundary-element method for an acoustic scattering problem*, Phil. Trans. R. Soc. Lond. A, **362**, 647-671.
- [9] L. He, S. Kindermann and M. Sini (2009) *Reconstruction of shapes and impedance functions using few far-field measurements*, J. Comput. Phys., **228**, 717-730.
- [10] Y.C. Hon and M. Li (2008) *A computational method for inverse free boundary determination problem*, Int. J. Numer. Meth. Eng., **73**, 1291-1309.
- [11] G. Inglese (1997) *An inverse problem in corrosion detection*, Inverse Problems, **13**, 977-994.
- [12] G. Inglese and F. Mariani (2004) *Corrosion detection in conducting boundaries*, Inverse Problems, **20**, 1207-1215.
- [13] V. Isakov (2009) *Inverse obstacle problems*, Inverse Problems, **25**, 123002 (18pp).
- [14] O. Ivanyshyn and R. Kress (2011) *Inverse scattering for surface impedance from phase-less far field data*, J. Comput. Phys., **230**, 3443-3452.
- [15] A. Karageorghis, D. Lesnic and L. Marin (2011) *A survey of applications of the MFS to inverse problems*, Inverse Problems Sci. Eng., **19**, 309-336.
- [16] R. Kress and W. Rundell (2001) *Inverse scattering for shape and impedance*, Inverse Problems, **17**, 1075-1085.
- [17] D. Lesnic, J.R. Berger and P.A. Martin (2002) *A boundary element regularization method for the boundary determination in potential corrosion damage*, Inverse Problems in Engineering, **10**, 163-182.
- [18] D. Lesnic and B. Bin-Mohsin (2012) *Inverse shape and surface heat transfer coefficient identification*, J. Comput. Appl. Math., **236**, 1876-1891.
- [19] L. Marin (2006) *Numerical boundary identification for Helmholtz-type equations*, Comput. Mech., **39**, 25-40.
- [20] L. Marin (2009) *Boundary reconstruction in two-dimensional functionally graded materials using a regularized MFS*, CMES Comput. Model. Eng. Sci., **46**, 221-253.
- [21] L. Marin (2010) *Regularized method of fundamental solutions for boundary identification in two-dimensional isotropic linear elasticity*, Int. J. Solids Struct., **47**, 3326-3340.
- [22] L. Marin, L. Elliott, P.J. Heggs, D.B. Ingham, D. Lesnic and X. Wen (2004) *Analysis of polygonal fins using the boundary element method*, Appl. Thermal Eng., **24**, 1321-1339.
- [23] L. Marin and A. Karageorghis (2009) *Regularized MFS-based boundary identification in two-dimensional Helmholtz-type equations*, CMC Comput. Mater. Continua, **10**, 259-293.
- [24] L. Marin, A. Karageorghis and D. Lesnic (2011) *The MFS for numerical boundary identification*

- in two-dimensional harmonic problems*, Eng. Anal. Boundary Elements, **35**, 342-354.
- [25] L. Marin and D. Lesnic (2003) *Numerical boundary identification in linear elasticity*, In: Fourth UK Conference on Boundary Integral Methods, (ed. S. Amini), Salford University, UK, pp 21-30.
- [26] L. Marin and L. Munteanu (2010) *Boundary identification in two-dimensional steady state anisotropic heat conduction using a regularized meshless method*, Int. J. Heat Mass Transfer, **53**, 5815-5826.
- [27] N. Mera and D. Lesnic (2005) *A three-dimensional boundary determination problem in potential corrosion damage*, Comput. Mech., **36**, 129-138.
- [28] C.D. Pagani and D. Pierotti (2009) *Identifiability problems and defects with the Robin condition*, Inverse Problems, **25**, 055007 (12pp).
- [29] W. Rundell (2008) *Recovering an obstacle and its impedance from Cauchy data*, Inverse Problems, **24**, 045003 (22pp).
- [30] P. Serranho (2006) *A hybrid method for inverse scattering for shape and impedance*, Inverse Problems, **22**, 663-680.
- [31] E. Sincich (2010) *Stability for the determination of unknown boundary and impedance with a Robin boundary condition*, SIAM J. Math. Anal., **42**, 2922-2943.
- [32] F.L. Yang, L. Yan and T. Wei (2009) *Reconstruction of part of boundary for the Laplace equation by using a regularized method of fundamental solutions*, Inverse Problems Sci. Eng., **17**, 1113-1128.
- [33] A. Zeb, D.B. Ingham and D. Lesnic (2008) *The method of fundamental solutions for a biharmonic inverse boundary determination problem*, Comput. Mech., **42**, 371-379.